Ann. Geophys., 31, 333–347, 2013
www.ann-geophys.net/31/333/2013/
doi:10.5194/angeo-31-333-2013

Annales Geophysicae
Open Access

Response of polar mesosphere summer echoes to geomagnetic disturbances in the Southern and Northern Hemispheres: the importance of nitric oxide

S. Kirkwood[1,2], E. Belova[1], P. Dalin[1], M. Mihalikova[1,2], D. Mikhaylova[1], D. Murtagh[3], H. Nilsson[1,2], K. Satheesan[1,*], J. Urban[3], and I. Wolf[1]

[1]Swedish Institute of Space Physics, Box 812, 98128 Kiruna, Sweden
[2]Graduate School of Space Technology, Luleå Technical University, Luleå, Sweden
[3]Department of Radio and Space Science, Chalmers University of Technology, Horsalsvagen 11, 412 96 Gothenburg, Sweden
[*]now at: National Center for Antarctic and Ocean Research, Goa, India

Correspondence to: S. Kirkwood (sheila.kirkwood@irf.se)

Received: 5 October 2012 – Revised: 3 February 2013 – Accepted: 7 February 2013 – Published: 27 February 2013

Abstract. The relationship between polar mesosphere summer echoes (PMSE) and geomagnetic disturbances (represented by magnetic K indices) is examined. Calibrated PMSE reflectivities for the period May 2006–February 2012 are used from two 52.0/54.5 MHz radars located in Arctic Sweden (68° N, geomagnetic latitude 65°) and at two different sites in Queen Maud Land, Antarctica (73°/72° S, geomagnetic latitudes 62°/63°). In both the Northern Hemisphere (NH) and the Southern Hemisphere (SH) there is a strong increase in mean PMSE reflectivity between quiet and disturbed geomagnetic conditions. Mean volume reflectivities are slightly lower at the SH locations compared to the NH, but the position of the peak in the lognormal distribution of PMSE reflectivities is close to the same at both NH and SH locations, and varies only slightly with magnetic disturbance level. Differences between the sites, and between geomagnetic disturbance levels, are primarily due to differences in the high-reflectivity tail of the distribution. PMSE occurrence rates are essentially the same at both NH and SH locations during most of the PMSE season when a sufficiently low detection threshold is used so that the peak in the lognormal distribution is included. When the local-time dependence of the PMSE response to geomagnetic disturbance level is considered, the response in the NH is found to be immediate at most local times, but delayed by several hours in the afternoon sector and absent in the early evening. At the SH sites, at lower magnetic latitude, there is a delayed response (by several hours) at almost all local times. At the NH (auroral zone) site, the dependence on magnetic disturbance is highest during evening-to-morning hours. At the SH (sub-auroral) sites the response to magnetic disturbance is weaker but persists throughout the day. While the immediate response to magnetic activity can be qualitatively explained by changes in electron density resulting from energetic particle precipitation, the delayed response can largely be explained by changes in nitric oxide concentrations. Observations of nitric oxide concentration at PMSE heights by the Odin satellite support this hypothesis. Sensitivity to geomagnetic disturbances, including nitric oxide produced during these disturbances, can explain previously reported differences between sites in the auroral zone and those at higher or lower magnetic latitudes. The several-day lifetime of nitric oxide can also explain earlier reported discrepancies between high correlations for average conditions (year-by-year PMSE reflectivities and K indices) and low correlations for minute-to-day timescales.

Keywords. Atmospheric composition and structure (Middle atmosphere – composition and chemistry) – Ionosphere (Ionospheric disturbances; Polar ionosphere)

1 Introduction

The coldest region of the Earth's atmosphere, the summer mesopause region at 80–95 km-height above the surface, forms over northern and southern polar latitudes during the

respective summer months. Here temperatures fall to below 150 K, forced well below radiative equilibrium by upward and equatorward winds which are caused by wave forcing of the global circulation. Temperatures become so low that ice clouds form, despite very low concentrations of water vapour. These mesospheric clouds can be observed from the ground during twilight as noctilucent clouds and have been studied for more than a century (e.g. Gadsden and Schröder, 1989). Their sensitivity to temperature and water vapour makes them a popular candidate for searching for possible signs of anthropogenic changes in atmospheric composition and radiative balance. Observations by satellite of increasing occurrence rates of mesospheric clouds have been used to argue for a long-term trend with slowly decreasing temperature at the summer mesopause (e.g. Shettle et al., 2009). On the other hand, ground-based observations of noctilucent clouds have not been able to discern any significant trend (e.g. Kirkwood et al., 2008a; Dubietis et al., 2010), nor have direct observations of temperature (e.g. Lübken, 2000). However, the number of available observations is limited. The proper quantification of trends really requires carefully calibrated quantitative observations covering all local times and repeated over several decades. Visual observations of noctilucent clouds are available for the longest period of time, but they are hard to calibrate, they are restricted to the twilight hours and they are often hampered by tropospheric clouds. Satellites have been available for a shorter period and provide observations only at fixed local times which change over the course of decades. Since mesospheric clouds can have a significant local-diurnal variation, this makes interpretation of satellite-based trends uncertain (e.g. Stevens et al., 2009, 2010).

An attractive alternative is to use radar, which offers the possibility of accurate calibration and complete local time coverage. The ice particles which form noctilucent clouds and the smaller sub-visual ice particles, which form first, coexist together within the lowest part of the Earth's ionosphere. Here the atmosphere is ionised by solar extreme-ultraviolet (EUV) radiation and by energetic particles from the magnetosphere, releasing free electrons and positive ions which interact with the ice particles. Although the details of this interaction are not fully understood, the result is a high level of small-scale structure in the electron density which is readily observed as strong radar echoes, known as polar mesosphere summer echoes (PMSE; for a review see Rapp and Lübken, 2004). The easiest parameter to measure for PMSE is the echo power. With care, it is possible to calibrate the measurements and to derive the reflectivity of the scatterers. Thanks to improvements in calibration methods, physically meaningful comparisons of PMSE strength between different radars at different locations and over periods of more than a decade have been made, with the hope of relating these to differences in temperatures, the latter being the most important parameter controlling the formation of ice particles. For example, Kirkwood et al. (2007) compared late-summer PMSE between Kiruna, Sweden (68° N, 19° E), and Wasa, Antarctica (73° S, 13° W), and found occurence rates to be very similar. This seemed to be consistent with the (limited) information then available, suggesting that summer mesopause temperatures at about 70° latitude were about the same in both hemispheres (Lübken et al., 1999). Nilsson et al. (2008) compared PMSE between Wasa and Davis, Antarctica (69° S, 78° E), and found about half the occurrence rates at Davis compared to Wasa, which was consistent with satellite indications of temperature differences at the time of those measurements between 69° S and 73° S. Latteck et al. (2008) compared PMSE for the years 2004–2006 between Resolute Bay, Canada (75° N, 95° W), Andenes, Norway (69° N, 16° E), and Davis, Antarctica (69° S, 78° W), and found occurrence rates of 18 %, 83 % and 38 %, respectively, with mean and maximum reflectivities also varying in the same order. For the same time interval, and the same detection threshold, Smirnova et al. (2010) found about a 75 % occurrence rate at Kiruna, which gives a consistent difference between Andenes/Kiruna/Wasa (all about the same) and Davis. Morris et al. (2009) considered longer data series from Davis and Andenes to confirm the lower rate of PMSE at Davis and found the difference consistent with satellite observations of slightly warmer temperatures in the Antarctic summer mesopause, compared to the same latitude in the Arctic. There remains, however, an inconsistency with the very low rates of PMSE occurrence at Resolute Bay. If temperatures in the Southern Hemisphere (SH) mesopause really are warmer than in the Northern Hemisphere (NH) at the same latitude, and temperature is the deciding factor for PMSE, then PMSE should be stronger at Resolute Bay than at all of Andenes, Kiruna and Wasa. Swarnalingam et al. (2009) have made careful checks on the reliability of PMSE reflectivity and occurrence rate estimates for Resolute Bay and found that they are indeed accurate; and applying the same methods for the similar radar at Yellowknife, Canada (62° N, 114° W), gives PMSE occurrence rates there similar to those at Andenes.

At the same time, studies of long-term (10–15 years) variations in PMSE reflectivity at Andenes (Bremer et al., 2009) and Kiruna (Smirnova et al., 2011) have shown a strong dependence on the level of geomagnetic disturbance (related to auroral activity). Reflectivity is expected to be affected not only by the properties of the ice particles (which depend on temperature) but also by other factors (see e.g. Varney et al., 2011, and references therein), such as those affecting small-scale structuring (e.g. turbulence), wave perturbations of the background temperature gradient (see also Dalin et al., 2012), and, perhaps most importantly, by electron density and electron density gradient. Yellowknife, Kiruna and Andenes in the Northern Hemisphere are all at latitudes within the auroral oval, Wasa is on the equatorward edge, and Davis and Resolute Bay are well poleward of the oval. The effects of energetic particle precipitation associated with auroral activity at PMSE heights can be expected to be greatest within the auroral oval (Codrescu et al., 1997). If we are to use

Table 1. Main characteristics of the radars used in this study. Geomagnetic coordinates are calculated using the online facility provided by Papitashvili (2012). Antenna effective area A_{Reff}, gain G_{T} and beam width θ_{T} are calculated on the basis of the dimensions and spacing of the antenna elements. Antenna parameters in parentheses applied during November and December 2011.

Radar	ESRAD	MARA
Geographic coordinates	67.88° N, 21.10° E	Wasa 73.04° S, 13.41° W Troll 72.01° S, 02.54° E
Height above sea level	295 m	Wasa 440 m Troll 1270 m
Geomagnetic latitude	64.9° N	Wasa 61.6° S, Troll 62.7° S
Geomagnetic midnight	21:28 UT (22:52 LT)	Wasa 02:11 UT (01:15 LT) Troll 01:35 UT (01:47 LT)
Operating frequency	52.0 MHz	54.5 MHz
Transmitter peak power P_{T}	72 kW	20 kW
Antenna effective area A_{Reff}	3740 m^2	540 m^2 (146 m^2)
Antenna gain G_{T}	31.5 dB	23.5 dB (18 dB)
Average feed loss L_{T}	0.5	0.8 (0.6)
Beam width θ_{T} (1-way, hwhm)	2.5°	6° (11°)
Nominal beam width $\pi/2G_{\mathrm{T}}^{0.5}$	2.40°	6.01° (11.6°)

PMSE to study hemispheric differences or long-term change in the temperature of the neutral atmosphere at the summer mesopause, we need first to understand better how the reflectivity responds to changes induced by energetic particle precipitation.

There is a larger offset between the magnetic and geographic poles in the Southern Hemisphere than in the Northern Hemisphere. As a result, observations from parts of Antarctica offer the possibility to study PMSE at high geographic latitude but relatively low geomagnetic latitude, reducing the effects of energetic particle precipitation. Observations from Antarctica have already been used to show that, during geomagnetically quiet conditions, PMSE reflectivities can, on average, be explained by ice-mass density together with electron densities produced by solar EUV radiation alone (Kirkwood et al., 2010b). In this study we particularly focus on how different responses to disturbance levels between a sub-auroral Antarctic site and an auroral Arctic site can indicate different mechanisms affecting PMSE strengths. We also look at how disturbance effects can affect conclusions drawn from comparisons between sites or over time.

2 MARA and ESRAD VHF radars

MARA (Moveable Atmospheric Radar for Antarctica) is a relatively small, 54.5-MHz radar which has made PMSE measurements in Antarctica during 5 summer seasons so far. From January 2006 to January 2011 MARA was operated during summer expeditions only at the Swedish/Finnish research stations Wasa/Aboa (the two stations are at the same site). Observations were made in 2007 from 23 January–5 February and 5–31 December, in 2008 from 1–31 January, in 2009 from 22–31 December, in 2010 from 1–27 January and 14–31 December, and in 2011 from 1–12 January. During 2011, MARA was moved to the Norwegian station Troll where it started operation on 23 November and is intended to operate year round for about 2 years. So the start and end of the SH PMSE season have been covered only once by MARA, during the 2011/2012 season. The basic configuration of MARA includes 20-kW peak transmit power, 3 receivers (6 since 2012) and an antenna array consisting of 3 groups, each of 16 dipoles (a smaller antenna array, consisting of 3 groups each of 4 three-element Yagis, was used 23 November 2011–4 January 2012). The main hardware characteristics are summarised in Table 1. Horizontal winds, echo aspect sensitivities and coherence times are measured using full correlation analysis, using the 3 antenna groups separately. Vertical wind (Doppler) and reflectivities are measured using the whole antenna (signals from the 3 groups are combined coherently in software).

ESRAD (ESrange RADar) is a moderately large, 52-MHz radar which has made PMSE measurements at Esrange, near Kiruna in Arctic Sweden since 1996. ESRAD operates continuously and provides complete coverage of the start and end of each of the seasons. Here we include measurements from 2006 to 2011 to compare with the same period of time as MARA observations. ESRAD has 72-kW peak transmit power, 6 receivers and an antenna array consisting of 6 groups, each of 48 five-element Yagi antennas (see Table 1 for more technical details). As at MARA, full correlation analysis is applied using separate antenna groups, while reflectivities and doppler are calculated using the whole antenna.

The receiver paths for both radars (including the whole path from antenna through the receivers) have been

calibrated by monitoring the daily variation of galactic noise, which is recorded as the noise level in the radar height profiles (Kirkwood et al., 2007, 2010a). Antenna feed losses for the MARA system (where the feed system is relatively simple) have been found by direct measurements on the various components. Tests with direct injection of known noise levels into the receiver system have been performed sporadically at both sites. This provides a check on feed losses at MARA and an estimate of feed losses at ESRAD. Comparison between Fresnel reflectivities at tropopause heights and values calculated from radiosonde profiles of atmospheric static stability provide a year-to-year check on transmitter power stability and losses on transmission (Kirkwood et al., 2011; Smirnova et al., 2011). Finally, MARA made PMSE observations in Kiruna, just 30 km from ESRAD in 2006, allowing cross calibration (Kirkwood et al., 2007).

Both MARA and ESRAD usually operate two or three measurement modes with different duty cycles and different height resolutions, generally switching between modes every minute. The measurements used here have been made with 8-bit complementary codes, with 4-μs (600 m) bit length, pulse repetition frequency (prf) 1300 Hz, 16 coherent integrations in hardware and 2 further coherent integrations in software (in total 49-ms integration time). Reflectivities and other parameters have been derived for each 1-min height profile and the results averaged for 1-h intervals before being used in the statistical study described in the rest of this paper.

3 Radar volume reflectivities

PMSE strengths are sometimes expressed in terms of signal-to-noise ratio, but this parameter depends on the characteristics of the radar making the measurements (transmitter power, antenna area, antenna and feed efficiency) and on the way in which the data has been collected (radar pulse length, receiver bandwidth, number of coherent integrations). For comparison between different radars at different locations it is important to use instead a parameter which is an intrinsic property of the atmospheric scatterers and which can be calculated from the echo power detected by the radar after correcting for all of those instrumental effects. The most commonly used measure for PMSE is volume reflectivity η, which is the radar cross section per unit volume of the atmosphere. If the scatter is isotropic, this can be found from the power scattered back to the radar. Two slightly different expressions have been applied in recent PMSE studies, i.e.

$$\eta = \frac{P_{\mathrm{RA}}}{P_{\mathrm{T}}} \frac{64(2\ln 2) r^2}{\pi L_{\mathrm{T}} V_{\mathrm{f}} A_{\mathrm{eff}} \Delta r}, \tag{1}$$

where P_{T} is power delivered to the antenna, P_{RA} is power due to atmospheric scatter received by the antenna, r is the distance to the scattering volume, Δr is the thickness of the volume element along the radar beam, A_{eff} is the effective area of the receiving antenna, L_{T} accounts for losses in the antenna feed on transmission (< 1) and V_{f} expresses the fraction of the scattering volume which is filled with scatterers (≤ 1).

Equation (1) is from Gage (1990) and has been used in earlier PMSE studies comparing ESRAD and MARA, e.g. Kirkwood et al. (2007). An alternative expression due to Hocking (1985) has been used by a number of other authors, particularly where different antenna areas have been used for transmission and reception. Combining Eqs. (28) and (33a) from the latter paper,

$$\eta = \frac{P_{\mathrm{RR}}}{P_{\mathrm{T}}} \frac{8\pi(2\ln 2) r^2}{L_{\mathrm{T}} L_{\mathrm{R}} G_{\mathrm{T}} A_{\mathrm{Reff}} {\theta_{\mathrm{B}}}^2 \Delta r}, \tag{2}$$

where P_{RR} is power due to atmospheric scatter detected at the receiver; G_{T} is the gain of the transmitting antenna; A_{Reff} is the effective area of the receiving antenna; L_{R} accounts for losses in the antenna feed on reception; θ_{B} is the half-power half-width of the volume contributing to the scatter, usually taken as the combined antenna beam on transmission and reception; and other parameters are the same as in Eq. (1). In this case,

$$\frac{1}{\theta_{\mathrm{B}}^2} = \frac{1}{\theta_{\mathrm{R}}^2} + \frac{1}{\theta_{\mathrm{T}}^2}, \tag{3}$$

where θ_{R} and θ_{T} are the one-way beam widths of the transmitting and receiving antennas, respectively.

Although Eqs. (1) and (2) appear to be rather different, substituting the (trivial) relations $P_{\mathrm{RA}} = P_{\mathrm{RR}}/L_{\mathrm{R}}$ and $\theta_{\mathrm{B}}^2 = \theta_{\mathrm{T}}^2/2$ (for the case when the same antenna is used for transmission and reception), and assuming $V_{\mathrm{f}} = 1$ and the (less obvious) approximate relation between beam width and gain,

$$\theta_{\mathrm{T}}^2 = \frac{\pi^2}{4G_{\mathrm{T}}}, \tag{4}$$

it can be seen that Eqs. (1) and (2) are identical. Although Eq. (4) is only an approximation, the values it gives for the MARA and ESRAD antennas are indeed very close to the values from antenna simulations (quoted in Table 1)

A problem in applying either Eq. (1) or Eq. (2) to measurements from radars with finite beam widths is that the scatter from PMSE is not completely isotropic. One way to account for this is to replace θ_{B} in Eq. (2) by an effective beam width θ_{eff} which depends on "aspect sensitivity" θ_{s}, an intrinsic property of the scatterers, and the true combined antenna beam width θ_{B}. Following Hocking et al. (1986),

$$\frac{1}{\theta_{\mathrm{eff}}^2} = \frac{1}{\theta_{\mathrm{s}}^2} + \frac{1}{\theta_{\mathrm{B}}^2}. \tag{5}$$

We can define a "normalised" or "narrow beam" volume reflectivity, which is the average reflectivity in the volume actually contributing to the scatter, i.e. the reflectivity which

would be measured by a radar with $\theta_B << \theta_s$ as follows:

$$\eta_N = \eta \frac{\theta_B^2}{\theta_{eff}^2}. \quad (6)$$

Using the interferometric capabilities of ESRAD and MARA it is possible to measure the effective beam width using full correlation analysis (Briggs, 1984; Holdsworth and Reid, 1995). In this case, however, only part of the antenna array is used for reception at each receiver. Each sub-array has a beam width θ_{RFCA}; thus the measured effective beam width is

$$\frac{1}{\theta_{effFCA}^2} = \frac{1}{\theta_s^2} + \frac{1}{\theta_T^2} + \frac{1}{\theta_{RFCA}^2}. \quad (7)$$

Combining Eqs. (3), (5) and (7) gives

$$\frac{1}{\theta_{eff}^2} = \frac{1}{\theta_{effFCA}^2} + \frac{1}{\theta_R^2} - \frac{1}{\theta_{RFCA}^2}. \quad (8)$$

In a recent study by Smirnova et al. (2012) using 11 years of PMSE measurements by ESRAD, it was found that half of the PMSE echoes have aspect sensitivity θ_s which is comparable to or slightly less than the ESRAD beam width. So θ_{eff} is significantly less than θ_B and the ratio η_N/η could be as high as a factor 2. The MARA radar has a broader beam than ESRAD, so this ratio can be expected to be higher. Figure 1 illustrates statistically the height distribution of effective beam width and the ratio η_N/η for the ESRAD and MARA observations used in this study. A complete description of the effective beam widths (and the aspect sensitivities which can be derived from these) is beyond the scope of the present work. For more details for PMSE at ESRAD we refer to Smirnova et al. (2012). Similar results are found for MARA, with no statistical variation of effective beam width with echo strength, but a distinct variation with height. Derivation of effective beam width from the radar measurements is subject to large random uncertainties for individual data samples, while corresponding estimates of η using Eq. (1) have rather small uncertainties. Since there is no statistical relation between aspect sensitivity and echo strength, we avoid introducing unnecessary random errors by using the mean profiles of η_N/η shown in Fig. 1 to calculate η_N.

Examples of volume reflectivities for two seasons of measurements are shown in Fig. 2. It is clear in Fig. 2 that the height of the PMSE layer behaved differently between MARA and ESRAD, at least for those two seasons. The same behaviour of PMSE height was reported and discussed following the first long season of observations with MARA in 2007/2008 (Kirkwood et al., 2008b). All subsequent seasons, particularly the even longer period of observations in 2011/2012 in Fig. 2, show the same behaviour, indicating that this is a stable characteristic of PMSE in the SH. For the present study we note only that it implies that SH PMSE

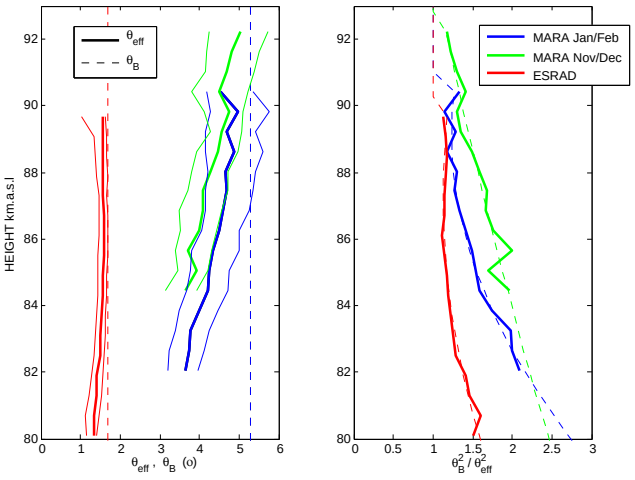

Fig. 1. Two-way antenna beam widths θ_B (dashed lines), median (thick lines) and quartile (thin lines) height profiles of effective beam width θ_{eff} (left-hand panel) and corresponding correction factors $\theta_B^2/\theta_{eff}^2$ to be applied to the volume reflectivity calculations (right-hand panel). Dashed lines in the left-hand panel are smooth curves fitted to the mean profiles of the correction factors. The fitted curves are used to correct reflectivities. See text for further details.

in the early season are generally found at rather higher altitudes than in the later season, which is the reason we consider separate height profiles for November/December and January/February, for example in Fig. 1.

4 PMSE response to magnetic disturbance

We can expect PMSE reflectivities to be strongly affected by electron density and electron density gradient. At polar latitudes, electron density depends on ionisation both by solar extreme-ultraviolet (EUV) radiation and by sporadic precipitation of high-energy electrons and protons from the magnetosphere. Whereas solar-produced ionisation is relatively easy to model, that due to precipitation is not because of the very variable characteristics of the source, both in time and in energy. However, the precipitation affecting PMSE heights will also cause ionisation at higher altitudes. The visible result of such precipitation is the aurora. At the same time, the increased electrical conductivity at heights above 100 km, and/or increased electric fields associated with the magnetospheric perturbations causing the particle precipitation, produce electric currents. The magnetic fields associated with these currents are then detected by magnetometers on the ground. Transient perturbations detected by magnetometers are regularly used to monitor the disturbed state of the ionosphere, generally quantified by the K index, which is a quasi-logarithmic measure of the degree of disturbance, derived for fixed 3-h time intervals.

To examine the response of PMSE to geomagnetic activity we use the K index from the magnetic observatory in Kiruna

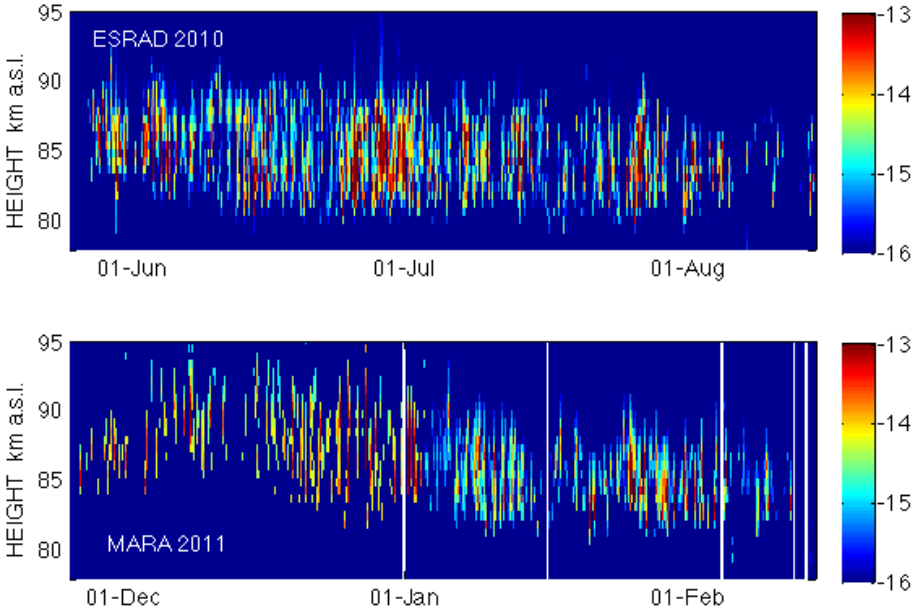

Fig. 2. Examples showing volume reflectivities (η_N) for two complete seasons of PMSE observations, the upper panel for ESRAD in the Arctic, the lower for MARA in Antarctica. Colour scale is the $\log_{10}$ of volume reflectivity, η_N.

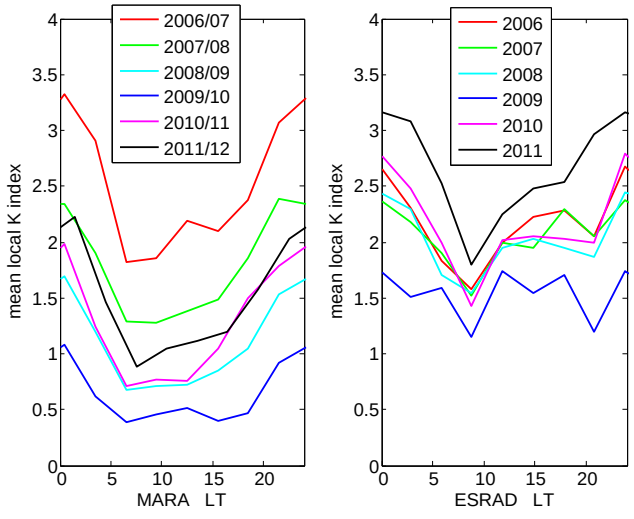

Fig. 3. Average K indices for each PMSE season (June/July for ESRAD, December/January for MARA) as a function of local (solar) time. K index used for MARA is from Leirvogur, Iceland, for ESRAD from Kiruna, Sweden. (Note that no measurements were made by MARA during the 2008/2009 season).

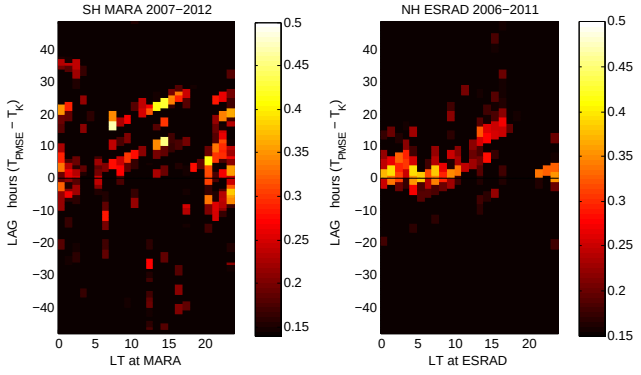

Fig. 4. Cross-correlation coefficients (colour scale) between local K index and PMSE reflectivity (maximum value each hour) as a function of local (solar) time and lag between K index and PMSE reflectivity. A positive lag means PMSE reflectivity increases after an increase in K index. Correlation coefficients are calculated separately for each season, and those with less than 95 % significance are set to zero before averaging.

for comparison with ESRAD. There is no magnetic observatory close to MARA, so we instead use the K index from Leirvogur, Iceland, which is the closest available to the magnetic conjugate location for MARA (Leirvogur is at magnetic latitude 65°, with magnetic midnight at 00:30 UT). Figure 3 illustrates the variation of the K indices from year to year and over local (solar) time during the main PMSE seasons at the two locations. Magnetic midnight is close to local solar midnight at both sites (see Table 1), so the magnetic-midnight maximum becomes a local-time midnight maximum. It is also clear that there have been more periods of low geomagnetic disturbance levels during the summer in the SH compared to the NH. Figure 4 shows the cross correlation between PMSE reflectivities (maximum over all heights for each hour) and the local K indices as a function of local time and lag between the PMSE observations and K index variations. For ESRAD, the highest correlations at most local

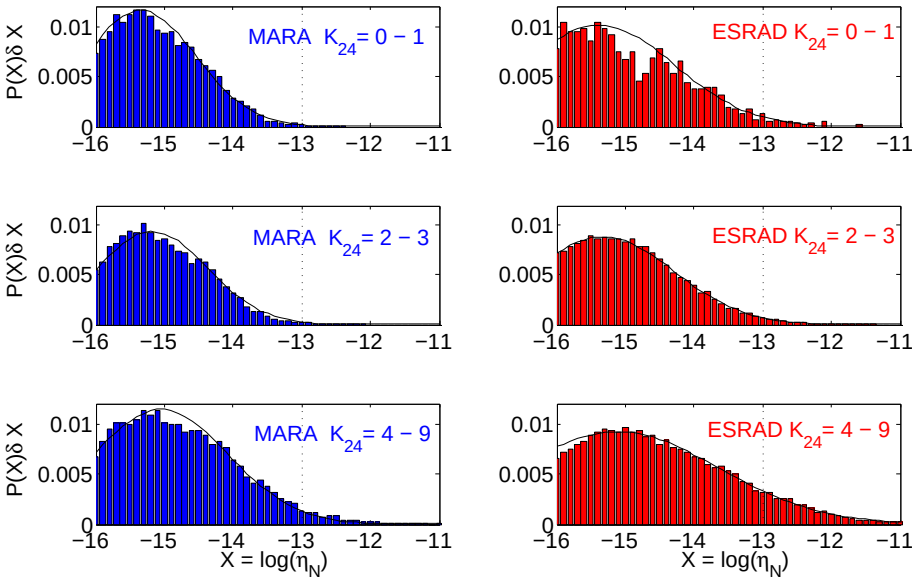

Fig. 5. Histograms showing the occurrence rate of PMSE as a function of volume reflectivity (η_N) for different levels of magnetic disturbance. Occurrence rates are based on 1-h averages – the months of June and July at ESRAD, December and January at MARA – and include observations for all heights (600-m resolution) between 78 and 100 km a.s.l. Black curves are fitted lognormal distributions with characteristics given in Table 2.

times are with zero lag; i.e. there is an immediate response of PMSE reflectivity to magnetic disturbance. However we note there is no sign of any response between 18:00 and 20:00 LT, and seemingly a delayed response (by 5–20 h) between 12:00 and 18:00 LT. For MARA, the highest correlation is almost always delayed by several hours, with some indication of an immediate response around midnight, but a substantial delay around midday.

The immediate response is clearly consistent with an effect of increased electron density and/or electron density gradient due to particle precipitation. The correlation coefficients are not high, reaching at most 0.4 at ESRAD in the early morning, corresponding to 16 % of the PMSE variability "explained" by variations in K index. However, given the indirect relation between K index and electron density, this might be expected. Also, the lack of an immediate response in the afternoon is consistent with the lower chance of particle precipitation in that time sector (see e.g. Codrescu et al., 1997). The generally delayed response at MARA is less easy to explain. The correlation is strongest during midday when solar EUV may be the dominant ionisation source. We will return to this feature later. For the moment we note only that, if we want to compare PMSE for different levels of magnetic activity, we need to consider not just the concurrent K index but the history of the K index during the preceding hours. So for further analysis we define a new index, K_{24}, which is simply the maximum value of the K index in the 24 h preceding and including the PMSE observation. This means, for example, that we consider conditions to be quiet only if the K index is low and has been low for at least a day.

Table 2. Details corresponding to the histograms and fitted curves in Fig. 5. First column lists the different conditions corresponding to the different histograms, second column the number of hours of observations available in each category. Third column gives the % of observations belonging to each category. The fourth and fifth columns list the parameters of the fitted lognormal distribution $P(X)dX = P_0 \exp(-(X-X_0)^2/W^2)$ where $X = \log(\eta_N)$ corresponding to dashed curves in the figure. The final column lists the maximum volume reflectivity observed in each category.

	Hours	%	X_o	W	max η_N
ESRAD $K_{24} = 0$–1	150	02	−15.4	2.4	2.3×10^{-12}
ESRAD $K_{24} = 2$–3	4343	58	−15.3	2.1	4.4×10^{-12}
ESRAD $K_{24} > 3$	2995	40	−15.1	4.4	2.2×10^{-10}
MARA $K_{24} = 0$–1	958	21	−15.3	1.1	3.9×10^{-13}
MARA $K_{24} = 2$–3	1915	42	−15.2	1.1	8.2×10^{-13}
MARA $K_{24} > 3$	1687	40	−15.0	1.9	2.5×10^{-11}

Figure 5 shows histograms of PMSE volume reflectivities separately for different levels of magnetic activity. The maximum detection threshold for PMSE volume reflectivity is $\eta_N = 10^{-16}\,m^{-1}$ for MARA and $\eta_N = 10^{-17}\,m^{-1}$ for ESRAD (it varies as the galactic noise level varies over the sidereal day). We show only the distribution above $\eta_N = 10^{-16}\,m^{-1}$ as comparisons for lower reflectivities are not meaningful. Table 2 gives an overview of the availability of PMSE observations for the different conditions, the characteristics of the lognormal distribution curves fitted to the histograms, and the maximum reflectivities. It can be seen that

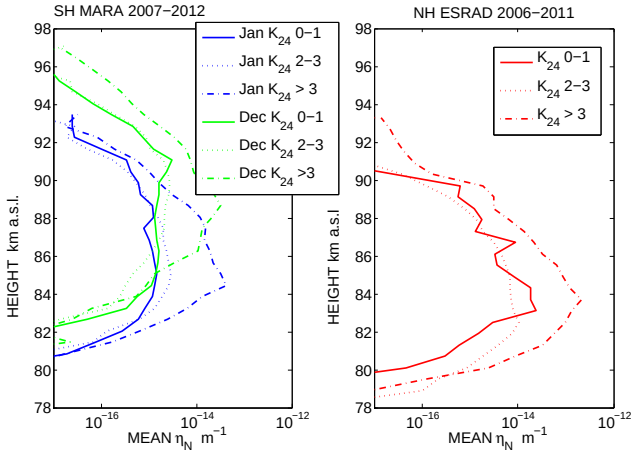

Fig. 6. Height profiles of mean PMSE volume reflectivity for different levels of magnetic disturbance. Means are based on 1-h averages, the months of June and July at ESRAD, December and January at MARA (separately for each month).Values below $\eta_N = 10^{-16}\,m^{-1}$ are set to zero before averaging.

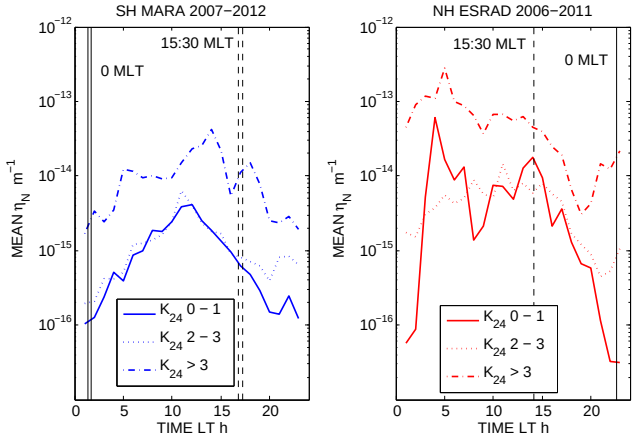

Fig. 7. Local-time dependence of mean PMSE volume reflectivity for different levels of magnetic disturbance. Means are based on 1-h averages, the months of June and July at ESRAD, December and January at MARA, with values below $\eta_N = 10^{-16}\,m^{-1}$ set to zero. Averages are over heights 80–90 km at ESRAD, 83–93 km at MARA.

the position of the peak of the distribution, and the width, increase with the level of magnetic disturbance, more so at ESRAD than at MARA. The tail of the distribution, above $\eta_N = 10^{-13}\,m^{-1}$ and the maximum reflectivities observed, increase dramatically for high levels of activity. The peak of the distribution is close to the same at both ESRAD and MARA, with a slight shift to higher reflectivities at higher K index levels, at both sites. The main difference between the sites is the greater width of the distribution, along with the much larger number of occurrences with high reflectivities at ESRAD.

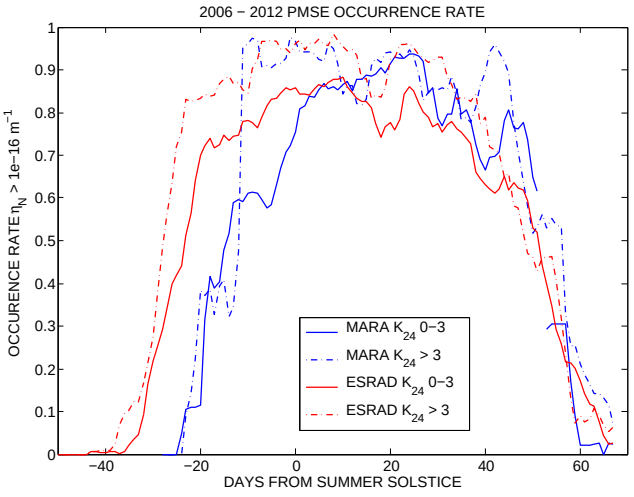

Fig. 8. Seven-day running mean occurrence rates of PMSE as a function of magnetic disturbance level. PMSE is defined as occurring if the one-hour average $\eta_N > 10^{-16}\,m^{-1}$ at any height.

Further illustrations of the influence of activity level are shown in Figs. 6 and 7, which show mean height profiles and local-time variations, respectively (all $\eta_N < 10^{-16}\,m^{-1}$ are treated as zero in the averages for a fair comparison between the two radars). In the height profiles, the effect of increasing magnetic disturbance levels is distinct only for $K_{24} > 3$. It affects the heights with highest reflectivities most, with less effect at lower and higher altitudes. The high-reflectivity tails of the distributions have a strong influence on the mean values such that the mean profiles for ESRAD are about an order of magnitude higher than for MARA. Referring to the local-time variations in Fig. 7 it is clear that the local-time variation shows considerable differences between the two locations. In the quietest conditions, close to midnight, reflectivities are very low, slightly lower at ESRAD than at MARA, consistent with lower electron densities due to EUV at the lower solar elevations around midnight at ESRAD. The increase in midnight-sector reflectivity as the activity level rises is only one order of magnitude at MARA but almost three orders of magnitude at ESRAD. There is a strong peak between 03:00 and 06:00 LT at ESRAD even in the quietest conditions, which is not present at all at MARA. The daily cycle, with a maximum close to midday and minimum at midnight, persists at MARA, whatever the disturbance level. At ESRAD it is replaced at the highest disturbance levels by a maximum around 05:00 LT and a minimum around 19:00 LT.

The behaviour over LT at ESRAD is mostly consistent with the known characteristics of energetic particle precipitation (Codrescu et al., 1997), with a maximum in the midnight and early-morning hours and a minimum in the afternoon. The early-morning peak, apparent even in quiet conditions, may be at least partly due to a peak in ice-particle densities at that time. For example Fiedler et al. (2011), using lidar measurements of noctilucent clouds over Andenes, have found

twice as much ice mass in the 03:00–05:00 LT time sector compared to the 10:00–24:00 LT sector. However, according to the results of Kirkwood et al. (2010b), relating ice-mass and electron densities to PMSE reflectivities, this should lead to a factor of only 2 difference between PMSE reflectivities between 03:00–05:00 LT and those at corresponding solar zenith angles in the afternoon (19:00–21:00 LT) if solar EUV is the only source of ionisation. Since the observed difference in reflectivities is an order of magnitude, it seems likely that this site is affected by energetic particle precipitation in the early morning even when K indices suggest that the situation is quiet. The behaviour around 15:30 MLT (marked on Fig. 7 by a vertical dashed line), however, cannot be explained by particle precipitation. This is the centre time of a minimum in the relevant particle fluxes – the minimum lasts several hours at low disturbance levels but reduces to about an hour at the highest disturbance levels (Codrescu et al., 1997). So we should not expect any increase in PMSE with increased magnetic activity around 15:30 MLT if the only cause is simultaneous energetic particle precipitation. Together with the delayed correlation in this time sector (Fig. 4), this suggests some other mechanism must be at work. The weak response of PMSE to $K_{24} > 3$ at heights above 88 km for ESRAD in Fig. 6 also suggests that energetic particle precipitation is not the only explanation since this source should give electron density enhancements which increase with height. (The lack of response at the base of the PMSE layer is likely simply due to the sharp base of the ice-particle layer.)

The local-time dependence of the reflectivity at MARA for $K_{24} > 3$ is not at all consistent with a direct response to energetic particle precipitation. As with ESRAD, the weak response at the upper heights in the PMSE layers is a further inconsistency with the expected effect of energetic particles. A possible explanation, for the weak response at the upper heights, the response at all LT at MARA, and the delayed response around 15:30 MLT at ESRAD, is that solar EUV remains the main ionising source at all levels of activity; but the underlying atmospheric composition is changed in response to magnetic disturbances, in particular the concentration of NO is enhanced, on a timescale of around one day. We will return to this question in the Discussion section.

Finally, we consider not average reflectivities but occurrence rates, for comparison with earlier studies, particularly from other radars. Figure 8 shows occurence rates for $\eta_N > 10^{-16}\,m^{-1}$, which is the limit of detectability at MARA, divided according to magnetic activity level. Figure 9 shows similar plots for $\eta_N > 10^{-15}\,m^{-1}$, which is the level chosen in a number of other studies. Clearly, the occurrence rate is dependent on both the level of magnetic disturbance and on the threshold chosen, as one lies just below the peak in the distribution, the other above. With the lower threshold, occurrence rates after the solstice at ESRAD and MARA are very similar (slightly lower at ESRAD in quiet conditions). They differ more in the early season, as PMSE starts about

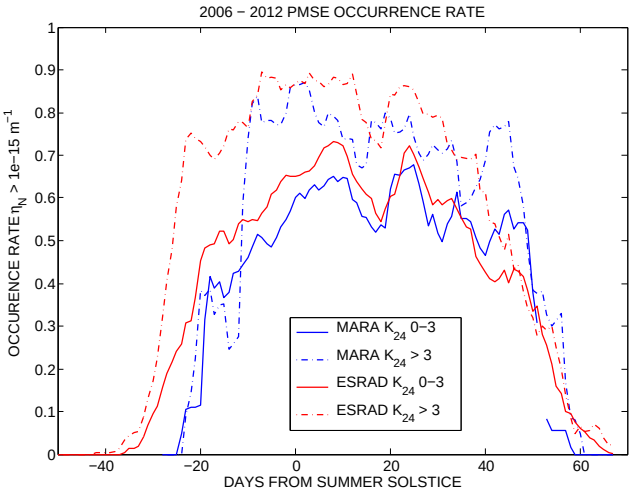

Fig. 9. As Fig. 8, but with a higher threshold to define PMSE occurrence, $\eta_N > 10^{-15}\,m^{-1}$.

10 days earlier at ESRAD. At the higher threshold, PMSE occurrence rates are substantially lower, particularly for quiet conditions, and they are on average slightly lower at MARA than at ESRAD.

As an aside, we mention that, although not shown here, all relationships have also been studied using the planetary Kp-index (which is derived from magnetic observatories at 40–60° latitudes in both hemispheres), and using the Kiruna K index also for MARA. The main features of Figs. 3–9 remain the same.

5 Discussion

The observations clearly show the importance of magnetic disturbance level for the distribution of PMSE reflectivities. In earlier publications, the influence of disturbance level on mean reflectivities has been recognised as important for year-to-year comparisons (e.g. Bremer et al., 2009; Smirnova et al., 2011), but the present study is the first time it has been considered in the context of comparing PMSE at different locations. Previous studies have generally concluded that the sensitivity to magnetic disturbance is due to direct increases of electron density by energetic particle precipitation, although it has been recognised that the correlation becomes very poor at high time resolution (minutes or hours) and, indeed, the possibility of other mechanisms has been suggested. In particular, Zeller and Bremer (2009) found evidence, using superposed-epoch analysis, that the increase of daily-average PMSE occurrence rate associated with magnetic activity was stronger the day after the maximum disturbance and persisted for several days. An explanation in terms of delayed precipitation of high-energy electrons from the magnetosphere in the days following magnetic storms was proposed. Such precipitation, however, should be strongest

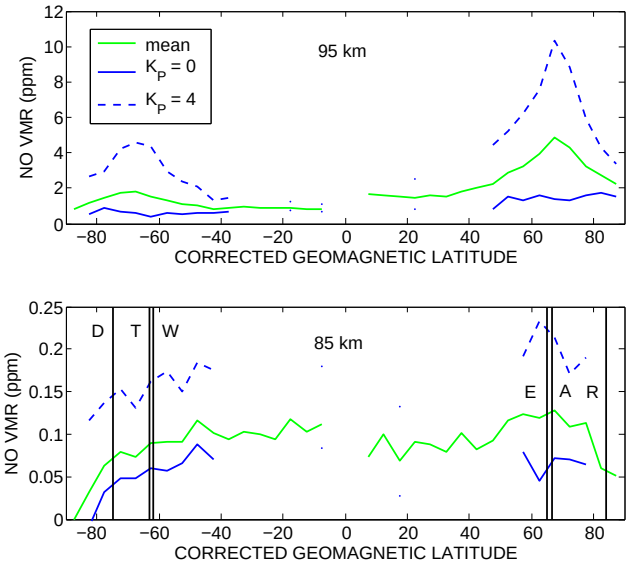

Fig. 10. NO volume mixing ratio, and its sensitivity to geomagnetic disturbance level, from the ODIN-SMR instrument, at two heights, 85 km and 95 km. NH estimates are for 50 days between 2004 and 2012 during the months June and July. SH estimates are based on days between December 2003 and January 2012 during the months December and January. Zonal means in 5° bins of corrected geomagnetic latitude are computed for each day and subsequently averaged to find the total mean (green line). Linear regression between the daily zonal means and mean planetary K index (K_P) for each measurement day are used to find the expected values at $K_P = 0$ (solid blue line)and $K_P = 4$ (dashed blue line). Vertical lines on the lower panel show the corrected geomagnetic latitudes of Davis (D), Wasa (W), Troll (T), Esrange (E), Andenes (A), Resolute Bay (R).

in the early morning hours (Codrescu et al., 1997). The present study is the first time the local-time dependence of the response has been examined including the possibility of a lagged effect. We have found (for MARA in Antarctica at most local times and for ESRAD in the Arctic in the post-noon sector) that there is a systematic lag between magnetic disturbance and PMSE-reflectivity increase, and a variation of the response over local time which is not consistent with a direct effect of energetic particle precipitation alone. We can expect PMSE reflectivity to depend on electron density and electron density gradient (e.g. Varney et al., 2011), and it is well known that these generally increase together as a result of energetic electron precipitation. It is also well known that the minor constituent nitric oxide (NO) has a strong influence on the electron density produced at PMSE heights by solar EUV radiation, specifically by the Lyman α spectral line (e.g. Barabash et al., 2012, and references therein). NO in the lower thermosphere in the auroral zone is well known to be strongly increased by auroral electron precipitation (energies up to a few keV) in association with magnetic disturbances, at least down to heights of 100 km (e.g. Barth et al., 2003). Medium-energy electrons (30 keV–2.5 MeV) are also precipitated into the atmosphere during geomagnetic disturbances and can be expected to lead to NO production at lower heights, 60–90 km, and over both auroral and sub-auroral latitudes (Codrescu et al., 1997). Whereas the direct electron density enhancement due to energetic electron precipitation has a lifetime of minutes, NO has a lifetime measured in hours or days, which means it can persist after the geomagnetic disturbance has ended, and it can be transported away from the latitudes, longitudes or heights where it is formed. This makes NO an obvious candidate to explain the delayed response of PMSE to magnetic disturbances.

In order to test whether NO enhancement due to geomagnetic activity might explain the PMSE behaviour, we have examined measurements made by the Sub-Millimeter Radiometre (SMR) instrument on the Odin satellite (Murtagh et al., 2002). Trace-gas measurements, including NO, covering the summer mesopause region, have been made by Odin-SMR since October 2003 (for a description of the measurement technique see Urban et al., 2007). Until May 2007, the relevant height range was covered for only about one day per month, but since then the coverage has increased to about 4 days per month. In total, 50 days of measurements are so far available for the NH summer months of June and July, 49 days for the SH summer months of December and January. Of these, 25 coincide with the PMSE measurements in the present study made by MARA in the SH, 33 with the ESRAD measurements in the NH. The NO concentration in the summer mesopause, particularly at high latitudes, is very low, making measurements difficult. The random uncertainty in the retrieval technique is also high, so zonal mean values (i.e. averaging over several satellite orbits) rather than individual profiles have to be used. Even using zonal means, at the latitudes we are most concerned with, 60–75°, the NO concentration is too low to be measured on 60 % of measurement days at 80 km-height. The situation is better at 85 km-height, with NO concentration too low to measure on only 15 % of days. By 95 km-height, measurements were possible on all of the days.

Figure 10 shows the mean over all available measurement days (green lines) for NO volume mixing ratio (v.m.r.), for retrievals centred at 85 ± 1 km and 95 ± 1 km heights, for June/July in the NH and December/January in the SH. Inspection of the retrieval diagnostics calculated by the SMR retrieval algorithm suggests an altitude resolution (full width at half maximum of the averaging kernel functions) of the order of 6–8 km in the height range 80–110 km. Measurements from every available orbit each day have been averaged in 5° bins of corrected geomagnetic latitude (Papitashvili, 2012). For days/latitudes/heights when the NO concentration was too low for valid retrievals to be made, the v.m.r. is set to zero before averaging over the whole data set (49 or 50 days), to avoid biasing the averages towards conditions of unusually high values. To examine the dependence on geomagnetic disturbance level, linear regressions have been made between NO v.m.r. and the mean of planetary K indices (K_P)) for

each latitude bin and each height over all available measurement days. The fitted regressions allow us to predict the most likely value of NO v.m.r. at any value of K_P. The blue lines show these predicted NO v.m.r. values for quiet ($K_P = 0$) and moderately disturbed ($K_P = 4$) conditions. The blue lines are shown only for latitudes where the correlation between NO v.m.r. and K_P is non-zero with 95 % confidence or better. There is a clear response of NO v.m.r. to geomagnetic disturbance level, for latitudes 50–80° N and 40–80° S, both at 85 km and at 95 km. At 95 km there are clear maxima in mean NO v.m.r. in the 65–70° geomagnetic latitude band in both hemispheres. At 85 km there is only a weak maximum in the 65–70° N band, but NO v.m.r. falls to very low values at latitudes higher than 80° in both hemispheres. There is also clearly a very steep vertical gradient in NO v.m.r. with values increasing by a factor of 20–40 between 85-km and 95-km heights.

The latitude variation of NO v.m.r. in Fig. 10 is very similar to what was found in the study by Siskind et al. (1997), which used modelling to explain observations of a high-latitude enhancement of NO in the summer mesopause region by the Halogen Occultation Experiment (HALOE) on the UARS satellite. Siskind et al. (1997) found that both direct production by medium-energy electrons (in their model, 15 keV) and downward diffusion from above 100 km – the main region of NO production by auroral electrons (2 keV in their model) – were needed to explain the observed NO enhancement at 89 km in the auroral zone. This was surprising since the mean atmospheric motion is upwards in the upper mesosphere at high latitudes during summer, so rather high values for the vertical diffusion coefficient were needed to counteract the upward mean circulation. However, the summer mesopause region is characterised by large-amplitude gravity waves and high levels of turbulence due to wind-shears and wave breaking (Lübken, 1997), and more recent estimates of effective diffusion coefficients (Grygalashvyly et al., 2012) suggest even higher values than those found necessary by Siskind et al. (1997).

Odin travels in a quasi-polar sun-synchronous orbit which nominally crosses the equator at 06:00 and 18:00 LT (in practice this has varied between 06:00–07:00 LT and 18:00–19:00 LT between 2003 and 2012). At our latitudes of interest, 60–75° N and S, the local time of the measurements is about 1 h closer to noon. There are about 15 orbits per 24 h. So the zonal means represent averages over 30 different longitudes, and for times ranging 06:00–08:00 LT and 16:00–18:00 LT. Averaging morning and evening passes separately (not shown) results in mean values for the high-latitude bands which are 20–40 % higher for morning than for evening, at both 85 km and 95 km. According to the study by Codrescu et al. (1997) energetic particle precipitation and NO production, increasing with the level of geomagnetic disturbance, can be expected, particularly for the 06:00–08:00 LT measurements. For quiet conditions, average NO levels at 95 km are the same for morning and evening, but for disturbed conditions ($K_P = 4$) they are up to 30 % higher. At 85 km, dividing the data into morning and evening results in estimates which are too uncertain to allow the K_P dependence to be found with reasonable confidence. Altogether, the sensitivity of NO to geomagnetic activity shown in Fig. 10 may be partly due to diffusion from higher altitude (which would be delayed) and/or to direct production by medium energy electrons (which would be both immediate and persistent).

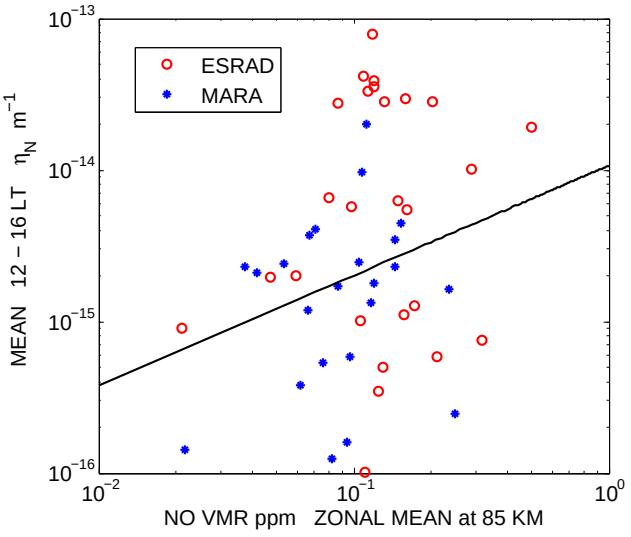

Fig. 11. Mean PMSE volume reflectivity, η_N, between 12:00 and 16:00 LT as a function of zonal mean NO measured by Odin-SMR on the same day. NO v.m.r. for the geomagnetic latitude band 60–65° S is used for MARA, 65–70° N for ESRAD.

Figure 11 compares PMSE volume reflectivities measured between 12:00 and 16:00 LT by ESRAD and MARA, with zonal mean NO v.m.r. at 85 km for corresponding geomagnetic latitudes (the band 60–65° S for MARA, 65–70° N for ESRAD) for each day when measurements are available. We choose the time 12:00–16:00 LT as this is when we hypothesise that NO rather than direct energetic electron precipitation is important in determining the background electron density. There is a weak positive correlation between NO v.m.r. and volume reflectivity (correlation coefficient 0.2 with 88 % confidence that it is non-zero). Given that the NO v.m.r. are zonal means and the variability with longitude may be large, that the NO measurements are not at the same local time, and that η_N depends not only on electron density but also on the characteristics of ice particles and turbulence, which can vary widely from hour to hour, we cannot expect a particularly close correlation. But the observed (weak) correlation is at least consistent with our hypothesis. Empirically it has been found that PMSE reflectivity increases roughly in proportion to electron density, at least for low levels of geomagnetic disturbance ($K_P < 3$) at Wasa (Kirkwood et al., 2010b), and we can expect electron density due to ionisation of NO by solar Lyman-α to increase as $[NO]^{0.5}$. Taking the

comparison a step further, the black line in Fig. 11 shows the fitted power-law relationship (linear regression to the logarithms of NO v.m.r. and η_N) assuming that NO v.m.r. is estimated accurately and the uncorrelated variability is in η_N. The exponent in the fitted power law is 0.7 (standard deviation 0.4), which is consistent with the value of 0.5 which we can expect. Comparing Figs. 10 and 7, we can conclude that the increase by a factor of 3–5 in NO v.m.r. between $K_P = 0$ and $K_P = 4$ is less than we would need to explain a 3–5-times increase in η_N from $K_{24} = 0$ to $K_{24} > 3$ around 15:30 MLT, if η_N is proportional to $[NO]^{0.5}$. This could be due to overestimating the very low NO v.m.r. during quiet conditions, when NO number density becomes very close to the noise level of the measurements. The climatology of Siskind et al. (1998) based on HALOE measurements (which have better sensitivity to low concentrations of NO) shows mean values at 85 km, slightly less than half of those we find with Odin-SMR. The larger change in η_N compared to the increase in NO v.m.r. could also be because η_N is more sensitive to electron density than simple proportionality. According to the theoretical predictions of Varney et al. (2011), η_N should be proportional to the square of electron density (i.e. to $[NO]^{1.0}$) for very low electron densities, decreasing to no dependence at high electron densities. Part of the increase in η_N, even close to 15:30 MLT, could also be due energetic electron precipitation. Even though the medium-energy precipitation should be at a minimum around 15:30 MLT in a statistical sense (Codrescu et al., 1997), it is not necessarily zero and there may be ionisation from higher energy (relativistic) electrons which are not represented in those statistics (see e.g. Horne et al., 2009).

To further test the order of magnitude of the changes in NO density at PMSE heights related to geomagnetic disturbances, and whether the delay in the correlation between η_N and $K_{24} = 0$ could be due to NO, requires accurate observations of the response of NO to energetic electron fluxes at the local scale and its development on timescales of hours to days. Such observations at PMSE heights and during the PMSE season have so far not been reported, but detailed local observations from Troll in Antarctica made between March and May 2008 have been reported by Newnham et al. (2011). Background NO v.m.r. between 70- and 85-km height was found to be 0.01–0.1 ppm. Increases in NO v.m.r. at 85 km were found, up to 0.3–0.5 ppm, maximising on average two days after maxima in geomagnetic disturbance level (diagnosed using the planetary Ap index). Corresponding daily mean K_P values for the disturbed days in question were between 3 and 4. So these values are consistent with the K_P dependence shown in Fig. 10. Newnham et al. (2011) found that the highest NO v.m.r. occurred below 80 km altitude and could be modelled as being produced by high-energy electrons (300 keV) penetrating as low as 70-km altitude. The amount of NO present built up slowly over a period of days, with production primarily during nighttime and loss during daytime. High amounts of NO were also shown to be produced by lower-energy electrons above 100 km, with no delay compared to the Ap index, but the possibility of downward diffusion to below 90 km was not considered.

So it seems clear that NO concentrations are increased at PMSE heights during geomagnetic disturbances. This can be by medium-energy electrons producing NO directly at PMSE heights, by relativistic electrons producing NO at lower heights followed by upward transport in the mean flow, or by lower-energy electrons at higher altitude followed by diffusion downward along the steep vertical gradient. The observed NO increases are of the same magnitude as the increases in η_N and can explain at least a substantial part of the delayed PMSE response to magnetic disturbances at MARA, and around 15:30 MLT at ESRAD (Fig. 4). Response through increased NO can also explain the weak sensitivity to K_{24} in the upper part of the PMSE layer, as ionisation of the minor constituent NO by Lyman α is the dominant source of electron density only below 88–90 km. Above that height (which will depend on the concentration of NO) ionisation of O_2 by the main part of the solar EUV spectrum dominates (e.g. Barabash et al., 2012).

If NO plays an important role in the strength of PMSE at sub-auroral latitudes (MARA), there is reason to expect that it also plays a significant role for the differences between different sites. The geomagnetic latitudes of several radar sites are marked by the vertical lines on the lower panel of Fig. 10. At ESRAD (E) and Andenes (A), for example, NO levels may be permanently enhanced due to the frequent particle-precipitation events in the auroral zone. Resolute Bay (R), at a magnetic latitude of 84°, is far poleward of the region of energetic particle precipitation, so local NO production cannot be expected. At the same time, during summer, the 24-h illumination by the Sun at the site's geographic latitude of 75° will effectively dissociate any background NO present, and NO levels can be very low, as Fig. 10 shows. Davis (D), at 69° geographic latitude, is at essentially the same geographic latitude as ESRAD and Andenes. But, since Davis is at 75° magnetic latitude, poleward of the auroral zone, less high-energy particle precipitation is expected such that average NO densities will be lower than at those sites (in agreement with Fig. 10). Altogether, we have to conclude that differences in PMSE reflectivities between sites may be as much an indication of mesopause NO densities as of mesopause temperatures. On the other hand, PMSE occurrence rates may still provide a measure of the presence or absence of ice particles, and therefore of temperature conditions, so long as detection thresholds are low enough for weak PMSE in the presence of solar ionisation alone, even in the presence of very low NO densities, to still be "visible".

6 Conclusions

We have compared magnetic K indices with PMSE reflectivities at ESRAD in Arctic Sweden (68° N, geomagnetic

latitude 65°) and MARA in Queen Maud Land, Antarctica (73°/72° S, geomagnetic latitude 62°/63°), using observations from 5 SH summer seasons and 6 NH summer seasons. ESRAD is located in the auroral zone, MARA at sub-auroral latitudes. We can draw the following main conclusions.

1. PMSE reflectivities at both locations have a lognormal distribution with a peak close to $\eta_N = 5 \times 10^{-16}\,m^{-1}$. The position of the peak increases only slightly with increasing levels of geomagnetic disturbance. The high-reflectivity tail of the lognormal distribution is more pronounced at ESRAD, particularly for high levels of disturbance ($K > 3$).

2. PMSE has the same occurrence rate at the two sites after solstice, with little dependence on magnetic activity level, provided that the threshold chosen for deciding on occurrence is below the peak at $\eta_N = 5 \times 10^{-16}\,m^{-1}$. Before the solstice, PMSE at MARA starts about 10 days later than PMSE at ESRAD and occurrence rates increase with increasing disturbance levels. This is in contrast to published studies comparing PMSE at Davis, Antarctica, with Andenes, Norway, which have found much weaker and less frequent PMSE in the SH throughout the season (Latteck et al., 2008; Morris et al., 2009).

3. If occurrence statistics are based on a threshold above the peak in the lognormal distribution, PMSE has a higher occurrence rate at ESRAD than at MARA, and occurrence rates are significantly higher in disturbed conditions than in quiet conditions. This may explain the much lower PMSE occurrence rates earlier reported from Davis and Resolute Bay (Latteck et al., 2008; Morris et al., 2009; Swarnalingam et al., 2009), compared to Andenes, where relatively high detection thresholds were applied ($\eta = 5 \times 10^{-15}\,m^{-1}$). The enhancing effect of geomagnetic disturbances can be expected to be much higher at the auroral zone site, Andenes, than at the polar cap sites, Davis and Resolute Bay.

4. PMSE reflectivity at MARA shows a delayed enhancement with increased disturbance level, a uniform response over local time, and a weak response in the upper heights of the PMSE layer, which are not consistent with enhancement due to immediate increases in electron density caused by energetic particle precipitation. A likely explanation is that a slow increase of NO, in response to local or non-local energetic particle precipitation in the magnetic night–morning sector, provides a basis for higher electron density to be produced by solar EUV radiation during the following day(s).

5. PMSE reflectivity at ESRAD shows mainly an immediate enhancement with increased magnetic disturbance level and a response which is strongest in the magnetic evening-night-morning sector, qualitatively consistent with what might be expected due to electron-density increases caused by energetic particle precipitation. However, delayed response near 15:00 LT and a weak response in the upper heights of the PMSE layer are not consistent with the latter mechanism and can be due to NO enhancement, as at MARA.

6. Zonal-mean NO v.m.r. at PMSE heights measured by the SMR instrument on the Odin satellite show a dependence on geomagnetic activity level which is qualitatively and quantitatively consistent with the PMSE response at MARA and at ESRAD in the afternoon sector. NO v.m.r. is lower at geomagnetic latitudes poleward of 75° than in the auroral and sub-auroral zones (55–75°), which is qualitatively consistent with the weaker PMSE reported from Davis, Antarctica, and Resolute Bay, Canada, compared to auroral zone sites. However, the difficulties of measuring the very low NO v.m.r. at the highest latitudes preclude a quantitative comparison.

While PMSE observations are certainly useful for monitoring the seasonal morphology of the cold summer mesopause, it will be difficult to use their occurrence rates and strengths to monitor long-term temperature changes or to determine average temperature differences between the hemispheres. PMSE reflectivity is simply too sensitive to magnetic activity conditions, which vary widely between seasons and affect different locations in different ways, and include delayed effects likely due to NO. Low PMSE detection thresholds, and careful correction for effects related to geomagnetic disturbances, will need to be used before any conclusions can be drawn about the underlying ice particles and the temperature conditions which determine their properties. Other properties of PMSE, which may be more closely related to the characteristics of mesospheric ice particles, such as aspect sensitivity and spectral width, should be explored as alternatives.

Acknowledgements. Measurements with MARA were part of the SWEDARP and FINNARP expeditions to Queen Maud Land, Antarctica, 2006/2007, 2007/2008, 2009/2010, 2010/2011, and 2011/2012. Operations at Troll are supported by the Norwegian Polar Institute. This research has been partly funded by the Swedish Research Council (grants 621-2007-4812 and 621-2010-3218), the Kempe Foundation and Knut and Alice Wallenberg's Foundation, Sweden. ESRAD is maintained and operated in collaboration with the Swedish Space Corporation, Esrange. Particular thanks are due to the polar logistics teams and to the Esrange staff for technical support. We thank also the Leirvogur Magnetic Observatory, University of Iceland, for providing K indices. Odin is a Swedish-led satellite project funded jointly by the Swedish National Space Board (SNSB), the Canadian Space Agency (CSA), the National Technology Agency of Finland (Tekes), the Centre National d'Etudes Spatiales (CNES) in France and through the 3rd party mission programme of the European Space Agency (ESA).

Topical Editor C. Jacobi thanks D. Newnham and one anonymous referee for their help in evaluating this paper.

References

Barabash, V., Osepian, A., Dalin, P., and Kirkwood, S.: Electron density profiles in the quiet lower ionosphere based on the results of modeling and experimental data, Ann. Geophys., 30, 1345–1360, doi:10.5194/angeo-30-1345-2012, 2012.

Barth, C. A., Mankoff, K. D., Bailey, S. M., and Solomon, S. C.: Global observations of nitric oxide in the thermosphere, J. Geophys. Res. (Space Physics), 108, 1027, doi:10.1029/2002JA009458, 2003.

Bremer, J., Hoffmann, P., Latteck, R., Singer, W., and Zecha, M.: Long-term changes of (polar) mesosphere summer echoes, J. Atmos. Solar-Terr. Phys., 71, 1571–1576, doi:10.1016/j.jastp.2009.03.010, 2009.

Briggs, B. H.: The analysis of spaced sensor records by correlation techniques, in: Handbook for MAP, vol. 13, pp. 166–186, Univ. of Ill., Urbana, 1984.

Codrescu, M., Fuller-Rowell, T., Roble, R., and Evans, D.: Medium energy particle precipitation influences on the mesosphere and lower thermosphere, J. Geophys. Res., 102, 19977–19987, 1997.

Dalin, P., Kirkwood, S., Hervig, M., Mihalikova, M., Mikhaylova, D., Wolf, I., and Osepian, A.: Wave influence on polar mesosphere summer echoes above Wasa: experimental and model studies, Ann. Geophys., 30, 1143–1157, doi:10.5194/angeo-30-1143-2012, 2012.

Dubietis, A., Dalin, P., Balčiūnas, R., and Černis, K.: Observations of noctilucent clouds from Lithuania, J. Atmos. Solar-Terr. Phys., 72, 1090–1099, doi:10.1016/j.jastp.2010.07.004, 2010.

Fiedler, J., Baumgarten, G., Berger, U., Hoffmann, P., Kaifler, N., and Lübken, F.-J.: NLC and the background atmosphere above ALOMAR, Atmos. Chem. Phys., 11, 5701–5717, doi:10.5194/acp-11-5701-2011, 2011.

Gadsden, M. and Schröder, W.: Noctilucent Clouds, Springer-Verlag, 1989.

Gage, K.: Radar observations of the free atmosphere: structure and dynamics, in: Radar in Meteorology, edited by: Atlas, D., chap. 28a, pp. 534–565, American Meteorological Society, Boston., 1990.

Grygalashvyly, M., Becker, E., and Sonnemann, G.: Gravity Wave Mixing and Effective Diffusivity for Minor Chemical Constituents in the Mesosphere/Lower Thermosphere, Space Sci. Rev., 168, 333–362, doi:10.1007/s11214-011-9857-x, 2012.

Hocking, W. K.: Measurement of turbulent energy dissipation rates in the middle atmosphere by radar techniques: A review, Radio Sci., 20, 1403–1422, doi:10.1029/RS020i006p01403, 1985.

Hocking, W. K., Ruester, R., and Czechowsky, P.: Absolute reflectivities and aspect sensitivities of VHF radio wave scatterers measured with the SOUSY radar, J. Atmos. Terr. Phys.., 48, 131–144, 1986.

Holdsworth, D. A. and Reid, I. M.: A simple model of atmospheric radar backscatter: Description and application to the full correlation analysis of spaced antenna data, Radio Sci., 30, 1263–1280, doi:10.1029/95RS00645, 1995.

Horne, R. B., Lam, M. M., and Green, J. C.: Energetic electron precipitation from the outer radiation belt during geomagnetic storms, Geophys. Res. Lett., 36, L19104, doi:10.1029/2009GL040236, 2009.

Kirkwood, S., Wolf, I., Nilsson, H., Dalin, P., Mikhaylova, D., and Belova, E.: Polar mesosphere summer echoes at Wasa, Antarctica (73 degrees S): First observations and comparison with 68 degrees N, Geophys. Res. Lett., 34, L15803, doi:10.1029/2007GL030516, 2007.

Kirkwood, S., Dalin, P., and Réchou, A.: Noctilucent clouds observed from the UK and Denmark – trends and variations over 43 years, Ann. Geophys., 26, 1243–1254, doi:10.5194/angeo-26-1243-2008, 2008a.

Kirkwood, S., Nilsson, H., Morris, R. J., Klekociuk, A. R., Holdsworth, D. A., and Mitchell, N. J.: A new height for the summer mesopause: Antarctica, December 2007, Geophys. Res. Lett., 35, L23810, doi:10.1029/2008GL035915, 2008b.

Kirkwood, S., Belova, E., Satheesan, K., Narayana Rao, T., Rajendra Prasad, T., and Satheesh Kumar, S.: Fresnel scatter revisited – comparison of 50 MHz radar and radiosondes in the Arctic, the Tropics and Antarctica, Ann. Geophys., 28, 1993–2005, doi:10.5194/angeo-28-1993-2010, 201a.

Kirkwood, S., Hervig, M., Belova, E., and Osepian, A.: Quantitative relation between PMSE and ice mass density, Ann. Geophys., 28, 1333–1343, doi:10.5194/angeo-28-1333-2010, 2010b.

Kirkwood, S., Mihalikova, M., Mikhaylova, D., Wolf, I., and Chilson, P.: Independent Calibration of Radar Reflectivities Using Radiosondes: Application to ESRAD, in: 20th Symposium on European Rocket and Balloon Programmes and Related Research, edited by: Ouwehand, L., vol. 700 of ESA Special Publication, pp. 425–429, 2011.

Latteck, R., Singer, W., Morris, R. J., Hocking, W. K., Murphy, D. J., Holdsworth, D. A., and Swarnalingam, N.: Similarities and differences in polar mesosphere summer echoes observed in the Arctic and Antarctica, Ann. Geophys., 26, 2795–2806, doi:10.5194/angeo-26-2795-2008, 2008.

Lübken, F.-J.: Seasonal variation of turbulent energy dissipation rates at high latitudes as determined by in situ measurements of neutral density fluctuations, J. Geophys. Res., 102, 13441–13456, 1997.

Lübken, F.-J.: Nearly zero temperature trend in the polar summer mesosphere, Geophys. Res. Lett., 27, 3603–3606, doi:10.1029/2000GL011893, 2000.

Lübken, F.-J., Jarvis, M. J., and Jones, G. O. L.: First in situ temperature measurements at the Antarctic summer mesopause, Geophys. Res. Lett., 26, 3581–3585, doi:10.1029/1999GL010719, 1999.

Morris, R. J., Klekociuk, A. R., Latteck, R., Singer, W., Holdsworth, D. A., and Murphy, D. J.: Inter-hemispheric asymmetry in polar mesosphere summer echoes and temperature at 69 deg latitude, J. Atmos. Solar-Terr. Phys., 71, 464–469, doi:10.1016/j.jastp.2008.09.042, 2009.

Murtagh, D., Frisk, U., Merino, F., Ridal, M., Jonsson, A., Stegman, J., Witt, G., Eriksson, P., Jiménez, C., Mégie, G., de La Noë, J., Ricaud, P., Baron, P., Pardo, J., Hauchecorne, A., Llewellyn, E., Degenstein, D., Gattinger, R., Lloyd, N., Evans, W., McDade, I., Haley, C., Sioris, C., von Savigny, C., Solheim, B., McConnell, J., Strong, K., Richardson, E., Leppelmeier, G., Kyrölä, E., Auvinen, H., and Oikarinen, L.: An overview of the Odin atmospheric mission, Can. J. Phys., 80, 309–319, 2002.

Newnham, D. A., Espy, P. J., Clilverd, M. A., Rodger, C. J., Seppälä, A., Maxfield, D. J., Hartogh, P., Holmén, K., and Horne, R. B.: Direct observations of nitric oxide produced by energetic electron precipitation into the Antarctic middle atmosphere, Geophys. Res. Lett., 38, L20104, doi:10.1029/2011GL048666, 2011.

Nilsson, H., Kirkwood, S., Morris, R. J., Latteck, R., Klekociuk, A. R., Murphy, D. J., Zecha, M., and Belova, E.: Simultaneous observations of Polar Mesosphere Summer Echoes at two different latitudes in Antarctica, Ann. Geophys., 26, 3783–3792, doi:10.5194/angeo-26-3783-2008, 2008.

Papitashvili, V.: Corrected Geomagnetic Coordinates and IGRF/DGRF Model Parameters, http://omniweb.gsfc.nasa.gov/vitmo/cgm_vitmo.html, 2012.

Rapp, M. and Lübken, F.-J.: Polar mesosphere summer echoes (PMSE): Review of observations and current understanding, Atmos. Chem. Phys., 4, 2601–2633, doi:10.5194/acp-4-2601-2004, 2004.

Shettle, E. P., DeLand, M. T., Thomas, G. E., and Olivero, J. J.: Long term variations in the frequency of polar mesospheric clouds in the Northern Hemisphere from SBUV, Geophys. Res. Lett., 36, 2803–2806, doi:10.1029/2008GL036048, 2009.

Siskind, D. E., Bacmeister, J. T., Summers, M. E., and Russell, III, J. M.: Two-dimensional model calculations of nitric oxide transport in the middle atmosphere and comparison with Halogen Occultation Experiment data, J. Geophys. Res., 102, 3527–3546, doi:10.1029/96JD02970, 1997.

Siskind, D. E., Barth, C. A., and Russel III, J. M.: A climatology of nitric oxide in the mesosphere and thermosphere, Adv. Space Res., 21, 1353–1362, 1998.

Smirnova, M., Belova, E., Kirkwood, S., and Mitchell, N.: Polar mesosphere summer echoes with ESRAD, Kiruna, Sweden: Variations and trends over 1997–2008., J. Atmos. Solar. Terr. Phys., 72, 435–447, 2010.

Smirnova, M., Belova, E., and Kirkwood, S.: Polar mesosphere summer echo strength in relation to solar variability and geomagnetic activity during 1997–2009, Ann. Geophys., 29, 563–572, doi:10.5194/angeo-29-563-2011, 2011.

Smirnova, M., Belova, E., and Kirkwood, S.: Aspect sensitivity of polar mesosphere summer echoes based on ESRAD MST radar measurements in Kiruna, Sweden in 1997–2010, Ann. Geophys., 30, 457-465, doi:10.5194/angeo-30-457-2012, 2012.

Stevens, M. H., Englert, C. R., Hervig, M., Petelina, S. V., Singer, W., and Nielsen, K.: The diurnal variation of polar mesospheric cloud frequency near 55° N observed by SHIMMER, J. Atmos. Solar. Terr. Phys., 71, 401–407, doi:10.1016/j.jastp.2008.10.009, 2009.

Stevens, M. H., Siskind, D. E., Eckermann, S. D., Coy, L., McCormack, J. P., Englert, C. R., Hoppel, K. W., Nielsen, K., Kochenash, A. J., Hervig, M. E., Randall, C. E., Lumpe, J., Bailey, S. M., Rapp, M., and Hoffmann, P.: Tidally induced variations of PMC altitudes and ice water content using a data assimilation system, J. Geophys. Res., 115, D18209, doi:10.1029/2009JD013225, 2010.

Swarnalingam, N., Hocking, W. K., Singer, W., and Latteck, R.: Calibrated measurements of PMSE strengths at three different locations observed with SKiYMET radars and narrow beam VHF radars, J. Atmos. Solar-Terr. Phys., 71, 1807–1813, doi:10.1016/j.jastp.2009.06.014, 2009.

Urban, J., Lautié, N., Murtagh, D., Eriksson, P., Kasai, Y., Loßow, S., Dupuy, E., de La Noë, J., Frisk, U., Olberg, M., Le Flochmoën, E., and Ricaud, P.: Global observations of middle atmospheric water vapour by the Odin satellite: An overview., Planet. Space Sci., 55, 1093–1102, doi:10.1016/j.pss.2006.11.021, special issue 2nd General Assembly of Asia Oceania Geophysical Society (2005): Highlights in Planetary Science, 2007.

Varney, R. H., Kelley, M. C., Nicolls, M. J., Heinselman, C. J., and Collins, R. L.: The electron density dependence of polar mesospheric summer echoes, J. Atmos. Solar-Terr. Phys., 73, 2153–2165, doi:10.1016/j.jastp.2010.07.020, 2011.

Zeller, O. and Bremer, J.: The influence of geomagnetic activity on mesospheric summer echoes in middle and polar latitudes, Ann. Geophys., 27, 831–837, doi:10.5194/angeo-27-831-2009, 2009.